Subthalamic deep brain stimulation sweet spots and hyperdirect cortical connectivity in Parkinson's disease

Authors:

Harith Akram FRCS (Neuro.Surg)[1,2], Stamatios N. Sotiropoulos PhD[5], Saad Jbabdi PhD [5], Dejan Georgiev PhD[1], Philipp Mahlknecht[1], Jonathan Hyam PhD FRCS (Neuro.Surg)[1,2], Thomas Foltynie PhD[1], Patricia Limousin PhD[1], Enrico De Vita PhD[6,7], Marjan Jahanshahi PhD[1], Marwan Hariz, MD, PhD[1,3], John Ashburner PhD[4], Tim Behrens PhD[4,5], Ludvic Zrinzo PhD FRCS (SN)[1,2]

Affiliations:

1. Unit of Functional Neurosurgery, Sobell Department of Motor Neuroscience and Movement Disorders, UCL Institute of Neurology, Queen Square, London, WC1N 3BG, UK
2. Victor Horsley Department of Neurosurgery, National Hospital for Neurology and Neurosurgery, Queen Square, London, WC1N 3BG, UK
3. Department of Clinical Neuroscience, Umeå University, Umeå, Sweden
4. Wellcome Trust Centre for Neuroimaging, UCL Institute of Neurology, Queen Square, London WC1N 3BG, UK
5. Centre for Functional MRI of the Brain (FMRIB), John Radcliffe Hospital, Oxford OX3 9DU, UK
6. Neuroradiological Academic Unit, Department of Brain Repair and Rehabilitation, UCL Institute of Neurology, Queen Square, London WC1N 3BG, UK
7. Lysholm Department of Neuroradiology, National Hospital for Neurology and Neurosurgery, University College London NHS Foundation Trust, London, UK

Corresponding author:

Harith Akram FRCS (Neuro.Surg)

Harith.akram.12@ucl.ac.uk

Unit of Functional Neurosurgery, UCL Institute of Neurology,

2nd Floor, 33 Queen Square, London, UK, WC1N 3BG

Fax: +44 (0) 20 3108 0142 Tel: +44 (0) 20 3108 0026

Running title: STN connectivity and DBS efficacy zones

Search terms: Diffusion weighted imaging (DWI), connectivity, Parkinson's disease (PD), subthalamic nucleus (STN), volume of tissue activated (VTA), hyperdirect pathway

Abbreviations:

AC	Anterior commissure
BEDPOSTX	Bayesian Estimation of Diffusion Parameters Obtained using Sampling Techniques X
BET	Brain extraction tool
CI	Confidence Interval
CON	Connectivity
DBS	Deep brain stimulation
DF	Degrees of freedom
DICOM	Digital Imaging and Communications in Medicine
DWI	Diffusion weighted imaging
EVs	Explanatory variables
FLIRT	FMRIB's linear image registration tool
FMRIB	Oxford Centre for Functional MRI of the Brain
FNIRT	FMRIB's non-linear image registration tool
FoV	Field of view
FSL	FMRIB's software library
GLM	General linear model
GPU	Graphics processing unit
HARDI	High angular resolution diffusion imaging
IPG	Implantable pulse generator
LC	Levodopa challenge
LEDD	L-DOPA equivalent daily dose
M1	Primary motor cortex
MMS	Mini-mental score
MNI	Montreal neurological institute
MPRAGE	Magnetization-prepared rapid gradient-echo
MPTP	1-methyl-4-phenyl-1,2,3,6-tetrahydropyridine
NHNN	National Hospital for Neurology and Neurosurgery
NIfTI	Neuroimaging Informatics Technology Initiative
PC	Posterior Commissure
PFC	Prefrontal cortex
SAR	Specific absorption rate
SD	Standard deviation
SE	Standard error
SMA	Supplementary motor area
SNR	Signal-to-noise ratio
SSEPI	Single-shot Echo Planar Imaging
STN	Subthalamic nucleus
TFCE	Threshold-free cluster enhancement
TMS	Transcranial magnetic stimulation
UPDRS	Unified Parkinson's disease rating scale
VBM	Voxel based morphometry
VTA	Volume of tissue activated
ZI	Zona incerta

Abstract

Objectives

Firstly, to identify subthalamic region stimulation clusters that predict maximum improvement in rigidity, bradykinesia and tremor, or emergence of side-effects; and secondly, to map-out the cortical fingerprint, mediated by the hyperdirect pathways which predict maximum efficacy.

Methods

High angular resolution diffusion imaging in twenty patients with advanced Parkinson's disease was acquired prior to bilateral subthalamic nucleus deep brain stimulation. All contacts were screened one-year from surgery for efficacy and side-effects at different amplitudes. Voxel-based statistical analysis of volumes of tissue activated models was used to identify significant treatment clusters. Probabilistic tractography was employed to identify cortical connectivity patterns associated with treatment efficacy.

Results

All patients responded well to treatment (46% mean improvement off medication UPDRS-III [$p<0.0001$]) without significant adverse events. Cluster corresponding to maximum improvement in tremor was in the posterior, superior and lateral portion of the nucleus. Clusters corresponding to improvement in bradykinesia and rigidity were nearer the superior border in a further medial and posterior location. The rigidity cluster extended beyond the superior border to the area of the zona incerta and Forel-H_2 field. When the clusters where averaged, the coordinates of the area with maximum overall efficacy was X=-10(-9.5), Y=-13(-1) and Z=-7(-3) in MNI(AC-PC) space. Cortical connectivity to primary motor area was predictive of higher improvement in tremor; whilst that to supplementary motor area was predictive of improvement in bradykinesia and rigidity; and connectivity to prefrontal cortex was predictive of improvement in rigidity.

Interpretation

These findings support the presence of overlapping stimulation sites within the subthalamic nucleus and its superior border, with different cortical connectivity patterns, associated with maximum improvement in tremor, rigidity and bradykinesia.

1 Introduction

Subthalamic nucleus (STN) high frequency stimulation is an established treatment in selected patients with advanced Parkinson's disease (PD) (Krack et al., 2003; Limousin et al., 1995; A. Williams et al., 2010). The STN is thought to comprise functional subdivisions implicated in motor, associative and limbic functions with degrees of overlap (Garcia-Garcia et al., 2016; Haynes and Haber, 2013; Lambert et al., 2012; Nakano et al., 1990; Nambu et al., 1996; 1997). The motor subdivision occupies the so-called 'dorsolateral' aspect; nevertheless, the most effective target location has been contended. Authors have argued that contacts within the 'dorsolateral-STN' give the biggest improvement in UPDRS-III(Johnsen et al., 2010; Weise et al., 2013; Wodarg et al., 2012); others have maintained that contacts 'dorsal' to the STN, in the zona incerta (ZI) area and Forel-H_2 field, have superior efficacy (Cintas et al., 2003; Godinho et al., 2006; Maks et al., 2009; Plaha, 2006; Vergani et al., 2007; Voges et al., 2002; Yelnik et al., 2003; Zheng et al., 2009). A third group found both locations, or border contacts to be equally effective (Garcia-Garcia et al., 2016; Hamel et al., 2003; Herzog et al., 2004; Lanotte et al., 2002; Yokoyama et al., 2001; Zonenshayn et al., 2004).

This discrepancy is attributed to several factors. One is reliance on surrogate markers such as microelectrode recording (Cintas et al., 2003; Godinho et al., 2006; Hamel et al., 2003; Lanotte et al., 2002; Maks et al., 2009; Vergani et al., 2007; Weise et al., 2013; Yokoyama et al., 2001; Zonenshayn et al., 2004) and non-specific atlas coordinates or deformable atlases (Garcia-Garcia et al., 2016; Godinho et al., 2006; Hamel et al., 2003; Lanotte et al., 2002; Maks et al., 2009; Vergani et al., 2007; Yelnik et al., 2003; Zonenshayn et al., 2004) to identify the STN borders, not readily

discernible on low or intermediate field MRI (Cho et al., 2010). Another is using postoperative CT instead of stereotactic-MRI to confirm contact location within the target, overlooking errors introduced by brain shift or image co-registration (O'Gorman et al., 2009; Petersen et al., 2010). Complicating matters further, is the STN's peculiar contour, double-oblique orientation and position within a junctional area where anatomical terms of location change, rendering localization description within the STN ambiguous (Hamani, 2004; Schaltenbrand et al., 1977; Yelnik et al., 2007). The term "dorsal", used when referring to the STN, is synonymous with "posterior" in the pons and "superior" in the thalamus (Coenen et al., 2008). Here we use unambiguous anatomical terms (superior/ inferior) to describe location within the STN.

Lastly, overlooking the volume of tissue activated (VTA) and only examining centre of ***active*** contacts location ignores the effect contacts adjacent to the nucleus might have on nuclear cell bodies dendrites as well as axons within the white matter outside the nucleus (Gradinaru et al., 2009; Hardman et al., 2002; Lumsden et al., 2015; Schmidt and van Rienen, 2012; Sotiropoulos and Steinmetz, 2007; Zhang and Grill, 2010) and limiting the comparison to the most effective contacts that landed in the chosen, predetermined target.

A proposed mechanism of action of STN-DBS is through interrupting synchronised oscillations between STN and cortex (Bergman et al., 1998; Brown, 2003; Eusebio et al., 2009; Hammond et al., 2007; Hirschmann et al., 2011; Lalo et al., 2008; Litvak et al., 2011; Shimamoto et al., 2013) possibly through modulation of hyperdirect pathways (Alexander and Crutcher, 1990; Alexander et al., 1990; Brown et al., 2001; DeLong, 1990; Kitai and Kita, 1987; Nambu et al., 1997; 1996; 2002; J. A. Obeso et al., 2008; Parent and Hazrati, 1995; D. Williams et al., 2002). The objectives of this study were to identify the optimal STN stimulation site separately for improvement in rigidity, bradykinesia and tremor; identify stimulation sites accountable for common side-effects encountered with STN-DBS one-year after surgery; and explore the cortical connectivity or ***fingerprint*** of stimulation volumes, through these hyperdirect pathways, in a bottom-up fashion, by proceeding stepwise through the following aims:

1. To create a ***group specific STN template*** by manually delineating, co-registering and averaging individual subthalamic nuclei

2. To screen all DBS contacts at amplitudes of 1,2,3 and 4 Volts for contralateral improvement in rigidity, bradykinesia and tremor; and emergence of side-effects
3. To generate VTA models for all DBS contacts at these amplitudes
4. To carry out a voxel based morphometry (VBM) style regression analysis of modelled VTAs and their associated efficacy and side-effect profiles
5. To use probabilistic tractography from modelled VTAs of all DBS contacts to predefined cortical areas excluding tracts passing through the thalamus and striatum and only including tracts passing through the internal capsule (hyperdirect pathway)
6. To generate a DBS-cortical connectivity matrix, using the output from the previous step, to test the predictive significance of cortical connectivity

2 Materials and methods

Ethical approval was granted by West London NHS REC (10/H0706/68). All participants provided written informed consent.

2.1 Patients

Twenty patients (4 female), who met UK Brain Bank criteria for idiopathic Parkinson's disease (Hughes et al., 1992), were included (Table1). Patients on the surgical waiting list for bilateral STN-DBS were recruited after selection by a multidisciplinary team of specialized movement disorders neurologists and functional neurosurgeons. All patients underwent formal neuropsychological assessment and structural brain MRI to rule out dementia and significant brain atrophy, respectively. Patients underwent L-DOPA challenge test during the routine selection process. Those with an improvement <25% on the UPDRS-III were excluded. Inclusion in the present study was limited to patients who could tolerate and had no contraindications to a prolonged 3T-MRI scan.

2.2 Preoperative diffusion MRI acquisition

This was performed on a 3T Siemens Magnetom Trio TIM Syngo MR-B17 using a padded 32-channel receive head coil to reduce discomfort and head motion.
Siemens' 511E-Advanced Echo Planar Imaging Diffusion WIP was used. In-plane acceleration was used (GRAPPA factor of 2) with partial Fourier 6/8. In plane resolution was $1.5\times1.5mm^2$ (Field of view $219\times219mm^2$, TR=12200ms, TE=99.6ms) and 85 slices were acquired with a 1.5mm thickness. Diffusion-weighting with $b=1500s/mm^2$ was applied along 128-directions uniformly distributed on the sphere and seven b=0s volumes were also acquired. To correct for distortions all acquisitions were repeated with a reversed phase encoding direction (left to right and right to left phase encode) giving a total of 270 volumes acquired ([128+7]×2). Total acquisition time was 62 minutes.

2.3 Surgical procedure and intraoperative-MRI

Bilateral DBS (3389 Medtronic lead) implantation was performed under GA using a stereotactic MRI-guided and MRI-verified approach without microelectrode recording (Leksell frame G, Elekta) as detailed in previous publications (Foltynie et al., 2011; Holl et al., 2010). Two stereotactic, pre-implantation scans were acquired, as part of the surgical procedure, to guide lead implantation; a T2-weighted axial scan (partial brain coverage around the STN) with voxel size of $1.0\times1.0mm^2$ (slice thickness=2mm) and a T1-weighted 3D-MPRAGE scan with a $(1.5mm)^3$ voxel size on a 1.5T Siemens Espree interventional MRI scanner. Three-dimensional distortion correction was carried out using the scanner's built-in module. Target for the deepest contact was selected at the level of maximal rubral diameter (~5mm below the AC-PC line). To maximising DBS trace within the STN, the target was often chosen 1.5-2mm posterolateral to that described by Bejjani (Bejjani et al., 2000). Stereotactic imaging was repeated following lead implantation to confirm placement. A dual channel implantable pulse generator (IPG) (Activa PC, Medtronic, Minneapolis, Minn., USA) was then implanted in the infra-clavicular region on the same day of lead implantation or within a week, as a staged procedure.

2.4 Outcome measures

2.4.1 DBS contact efficacy and side-effect profile screening

DBS efficacy and side-effects screening was performed one-year from surgery. Medications were withdrawn for twelve-hours before assessment. DBS was switched off and after a five to ten-minute washout period, hemi-body (upper limb) rigidity, bradykinesia and tremor scores were assessed and rated from 0-4 (0=normal, 1=slight, 2=mild, 3=moderate and 4=severe). Once baseline scores were documented, all contacts were screened one at a time using monopolar stimulation in four stimulation sessions with amplitudes of 1, 2, 3 and 4 volts, frequency of 130Hz and pulse width of 60μs until the effect was established. A washout period was allowed between stimulation sessions until baseline was reached. Scores were reassessed for every session whilst evaluating the emergence and progression of stimulation-related side-effects (i.e. facial pulling, dysarthria, diplopia and paraesthesia). An example screening sheet is provided in supplementary material.

2.4.2 DBS-VTA modelling

SureTune® (Medtronic Inc. Minnesota), a DBS therapy planning platform was used to model VTAs around individual contacts and to manually delineate STN volume meshes. The VTAs were created based on homogeneous finite element simulations of the distribution of the electric potential together with coupled axon cable models. Axon models were composed of 21 nodes, with a diameter of 2.5 μm and oriented in the vicinity of the lead in a perpendicular orientation. Specific VTA thresholds were calculated for every electrical setting taking in consideration the specific stimulation configuration, amplitude and pulse width as described by Åström and colleagues in order to generate DBS therapy VTA (Åström et al., 2015). Patient-specific tissue conductivity and patient-specific axon orientations were not considered. Intraoperative (pre- and post-implantation) stereotactic scans were co-registered. Scans were first manually aligned to pre-implantation MPRAGE scan before running automated co-registration with a restricted volume of fusion centred around the diencephalon/ mesencephalon. This was carried out to minimise registration error resulting from eventual brain shift incurred during surgery, despite minimal brain shift with our surgical technique (Petersen et al., 2010). Registration accuracy was carefully inspected and the process iterated if necessary.

Pre-implantation T2-weighted stereotactic scans were used to generate STN meshes. Two experienced practitioners (HA a functional neurosurgeon and PM a movement disorders neurologist) carried out the process independently with <15% interrater

variability in identifying the boundaries of the STN across patients. The post-implantation MPRAGE was used to fit the DBS lead model within the MRI artefact produced by the leads. Individual VTAs were then generated around each DBS contact with voltages of 1, 2, 3 and 4 volts resulting in 32 VTAs per patient.

2.5 Image Pre-processing

Pre-implantation MPRAGE scans were brain extracted using *BET* (Brain Extraction Tool, FSL v5.0) (Smith, 2002). A two-step procedure was used to register native scans to the MNI152 standard-space T1-weighted average structural template image (1mm resolution) (Grabner et al., 2006). The first step employed a linear (affine) transformation using *FLIRT* (FMRIB's Linear Image Registration Tool) using 12 degrees of freedom (Jenkinson et al., 2002; Jenkinson and Smith, 2001). The output from this step was used to execute non-linear registration (second step) using *FNIRT* (FMRIB's Non-Linear Image Registration Tool) (Andersson et al., 2007). This process produced individual native-to-standard (MNI space) non-linear warp fields which were then applied to the STN and VTA volumetric meshes acquired from SureTune to transform all volumes to standard space.

2.5.1 Diffusion pre-processing

All diffusion weighted imaging (DWI) scans (with accompanying b=0 scans) were converted to NIfTI volumes and the diffusion gradient direction values and vectors were extracted using *Volconv* (MJ White, NHNN Neuroradiology Department, London UK).

Opposite phase-encode blips acquisition pairs were used to estimate the susceptibility-induced off-resonance field (Andersson et al., 2003) as implemented in FSL (Smith et al., 2004) and the two images were combined into a single corrected one using *Topup* (FSL v5.0), a tool for estimating and correcting susceptibility induced distortions prevalent in SSEPI DWI. Eddy (FSL v5.0) was then used to correct for eddy current distortions and subject movement (Andersson and Sotiropoulos, 2016).

Patient averaged distortion corrected b=0 volume was registered to brain extracted structural image in native patient space (pre-implantation MPRAGE) with *Flirt* (FSL

v5.0) using linear registration with six degrees of freedom. The resultant transformation matrices were applied with the warp fields previously generated using non-linear registration between the structural in native patient space and the standard MNI152-1mm space producing diffusion-to-standard space warp fields and their corresponding inversions.

BedpostX (FSL v5.0) was then used to estimate fibre orientations. Up to three crossing fibres were estimated in each brain voxel using model 2 and graphics processing unit (GPU) parallelization (Hernandez et al., 2013; Jbabdi et al., 2012). *Probtrackx* was used on these estimates to obtain global connectivity (i.e. the probability of the existence of a path through the diffusion field between any two distant points, a surrogate measure of anatomical connectivity) (Behrens et al., 2007). Using the obtained transformations to and from standard space, tractography protocols and masks were defined in MNI space.

2.6 Analysis

2.6.1 Model of VTAs and efficacy scores

Group-average, bilateral STN templates and total VTA areas were generated from standardised (MNI space) individual STN volumes and DBS contacts VTAs using *Fslmaths* (FSL5.0) (see figures1 and 2).

Right sided individual contact VTAs were lateralised to the left by swapping the x axis (x, y, z > -x, y, z) using *Fslswapdim* (FSL5.0). All VTAs were then merged using *Fslmerge* (FSL5.0) into a 4D data file. In each voxel, each of the VTAs (one for each of the 32 different stimulation conditions) was modelled as a linear combination of efficacy scores, and side-effects (0=absent, 1=transient or 2=persistent) within subject. A general linear model (GLM) was created with efficacy and side-effects variables to test against each voxel in corresponding VTAs in a single-group average design (each variable was tested individually). This analysis was carried out for each subject independently. The variables were demeaned and single group t-test with threshold-free cluster enhancement (TFCE) was used as test statistic (Smith and Nichols, 2009). Nonparametric permutation inference approach, similar to that commonly used for VBM and fMRI timeseries analysis, was carried out for each voxel using *Randomise* (FSL5.0) with 5000 permutations to build up the null distribution to test against as previously described (Winkler et al., 2014). Raw t-stat (t

statistic) images were then masked by the significant voxels from thresholded (α=0.05) t-stat images, also corrected for multiple comparisons. The resultant images from each subject were combined to form a group average. Cluster-based inference using *Cluster* (FSL5.0) was carried out to extract the clusters and local maxima in outputs.

2.6.2 Tractography

Probabilistic tractography was generated in ProbtrackX2 GPU version (Behrens 2007) (Hernandez-Fernandez et al., 2016) (FSL5.0) (number of samples=5000, curvature threshold=0.2, step length=0.5mm subsidiary fibre volume fraction threshold=0.01) (Jbabdi and Johansen-Berg, 2011).

The combined (total) VTA areas were used to generate tractography (in MNI space) for the left and right hemispheres; additionally, tracts were generated from combined efficacy clusters instigating improvement in bradykinesia, tremor and rigidity as generated from the voxel-based morphometry (VBM) style DBS-contact VTA analysis in *Randomise* (FSL5.0).

Waypoints were used in the internal capsule to isolate the streamlines to three cortical target areas; (1) primary motor cortex (M1 [Brodmann's area 4]), (2) supplementary motor area (SMA) [Brodmann's area 6] and (3) prefrontal cortex (PFC). CSF termination and mid-sagittal exclusion masks were applied to exclude false positive streamlines and commissural tracts respectively. To improve connectional contrast between the three targets, each of them was used as a target, while the other two were used as exclusion masks. For instance, to track the STN-M1 pathway, M1 was used as target, while SMA and PFC were used as exclusion masks. This ensured that the tracked connection contained paths connecting STN to M1, and at the same time not connecting STN to any of the other two targets. Similarly, for the other two target regions.

2.6.3 DBS-Cortical connectivity

A connectivity matrix was generated between all seed points in the combined (total) VTA area mask and all points in the cortical target masks (i.e. M1, SMA and PFC) using the output from tractography. The streamline counts for each voxel were normalised by the total number of streamlines reaching all targets to acquire a proportional measure. A t-statistic was used to calculate the connectivity within the

individual DBS-contact VTAs (inside) versus the connectivity outside the contact VTAs but within the combined (total) group average VTA and this value was used in subsequent regressions (denoted as CON). This value effectively reflected connectivity of voxels activated in a certain stimulation condition, using connectivity in inactive STN voxels as a baseline. An in-house Matlab (Mathworks Inc.) script was used to test the relationship between the cortical connectivity of individual DBS-contact VTA voxels and the improvement in efficacy associated with each DBS-contact VTA. To account for the effect of VTA volume and stimulation amplitude on efficacy, these factors were used as nuisance covariates in the regression analysis. Efficacy for alleviation of a particular symptom was then modelled as a linear combination of the connectivity values to each of the three target areas, VTA volume and stimulation voltage, as shown below. Alleviation of three symptoms was individually explored (tremor, bradykinesia and rigidity). All the explanatory variables (EVs) were normalised (demeaned and standard deviation made equal to 1), so that

$$\boldsymbol{Efficacy = b_0 + b_1 \times CON_{VTA \rightarrow M1} + b_2 \times CON_{VTA \rightarrow SMA} + b_3 \times CON_{VTA \rightarrow PFC} + b_4 \times VOLTAGE + b_5 \times VTA\_VOLUME}$$

CON: connectivity; VTA: volume of tissue activated; M1: primary motor area; PFC: prefrontal cortex; SMA: supplementary motor area, b_0-b_5: unknown model parameters.

3 Results

3.1 Patients

Scanning proceeded with no adverse effects. The mean pre-operative mini-mental score (MMS) was 29.6 (SD=0.6, Range=2). One patient had tremor-dominant PD without motor fluctuations. Six patients had no significant tremor and were therefore excluded from the tremor VTA efficacy and cortical connectivity analysis, but included in the rigidity and bradykinesia analyses. There was no surgical morbidity or mortality and all DBS leads landed within a mean (SD) of 0.8 (0.4) mm from the planned target. Patient demographics, improvement in UPDRS-III following L-DOPA administration (L-DOPA challenge, preoperatively), improvement in UPDRS-III one-

year from surgery with DBS ON and OFF medications and change in L-DOPA equivalent daily dose are shown in table1.

3.2 VTA Modelling

Group average, statistically significant clusters correlated to stimulation efficacy and side-effect EVs within and around the STN are shown in Figures2 and 3. Improvement in bradykinesia, rigidity and tremor with DBS was associated with VTA clusters in the posterior, superior and lateral STN with the bradykinesia and rigidity areas extending to the superior border and being more medial and posterior than that of tremor. The three clusters were averaged into a single area in the superior and lateral STN with maximum intensity at X=-10(-9.5) Y=-13(-1) and Z=-7(-3) in MNI (AC-PC) space. Facial pulling was associated with VTA cluster in the region of the corticobulbar fibres. Acute dysarthria was associated with VTA cluster in the internal capsule. Diplopia was associated with the VTA cluster in the region of the mesencephalic oculomotor nerve fibres in the tegmentum. Paraesthesia was associated with the VTA cluster in the mid-portion and inferior STN. See Table2 for cluster volumes and MNI coordinates.

3.3 Tractography

3.3.1 Tractography from combined, group average, entire VTA area

Six tracts were generated for each patient starting from the entire average VTA seed mask and ending in one of the predefined cortical targets in both hemispheres. Tracts to M1 ended mostly medially extending to the hand area. Group averages were produced for each tract class. The resulting six group average tracts are shown in Figure4.

3.3.2 Tractography from bradykinesia, rigidity and tremor efficacy clusters

Eighteen tracts ([3 efficacy seed clusters × 3 cortical targets] × 2 hemispheres) for each patient were generated using seed masks corresponding to efficacy clusters in the STN as shown in Figure3. Tract group averages were again produced for each tract class (i.e. individual efficacy clusters to M1, SMA and PFC). Only tracts ending in the medial aspect (superior frontal gyrus) of M1, SMA and PFC survived. This is shown in Figure4.

3.4 DBS-Cortical connectivity analysis

Rigidity, bradykinesia and tremor had different VTA-cortical connectivity predictive profiles. Table3 shows which model parameters significantly contribute to predicting efficacy for each symptom. In the case of rigidity, connectivity to SMA (b_2~32 [p=0.0006]) and PFC (b_3~26 [p=0.005]) were highly significant. The effect was about half of that explained by voltage (b_4~53 [p<0.0001]). For bradykinesia only connectivity to SMA was highly significant (b_2~23 [p=0.005]). The effect was about two-thirds of that explained by voltage (b_4~34 [p=0.001]). In the case of tremor, connectivity to the primary motor area was significant (b_1~27 [p=0.04]). The effect was about a third of that explained by voltage (b_4~80 [p<0.0001]).

Figure5 shows the relationship between connectivity and efficacy for different stimulation amplitudes. Even if stimulation amplitude is a strong predictor of efficacy in all cases, the effect of connectivity can be also seen, particularly for rigidity and bradykinesia. For rigidity we can observe an upward trend for the efficacy as a function of the median connectivity to SMA. Particularly for intermediate voltages (2 and 3 Volts), being at an STN sub-region with higher connectivity to SMA leads to higher efficacy in alleviating rigidity. For bradykinesia, there is not a clear trend for high voltages (3 and 4 volts), but low/medium stimulation (1 and 2 volts) seems to benefit from being at a location with a high SMA connectivity. Thus, when voltage is low, exact contact location within the STN really matters. The profiles for tremor are much noisier and voltage amplitude clearly determines efficacy in this case.

4 Discussion

Voxel based statistical analysis of volumes of tissue activated, at increasing amplitudes, around individual DBS contacts, one year after STN DBS was used in 20 patients with Parkinson's disease (14 patients in the case of tremor) to (1) map out statistically significant clusters in the STN area, reflecting efficacy and side effects zones; (2) generate probabilistic tractography streamlines (hyperdirect pathways) from said volumes to predefined cortical areas [M1, SMA and PFC] and (3) identify the pattern of cortical connectivity that predicts response to treatment.

Appropriately selected patients responded well to DBS with reduction in LEDD and improvement in UPDRS-III both ON and OFF medications one-year post op (Table1).

4.1 Efficacy and side-effects clusters in the STN region

Using a statistical analysis approach akin to that used in voxel based morphometry, distinct clusters in the STN corresponding to improvement in rigidity, bradykinesia and tremor are demonstrated (Figures 2 and 3). All clusters are in the supero-lateral (motor) STN with overlapping bradykinesia and rigidity clusters. The tremor cluster is central within the supero-lateral STN whilst rigidity and bradykinesia appear to be more medial, posterior and superior. The rigidity cluster is the largest of the three and extends beyond the STN into the subthalamic region in the area of rostral ZI and Forel-H_2 field (pallido-thalamic fibres) whilst the bradykinesia cluster does not extend beyond the STN border (Schaltenbrand et al., 1977). The average cluster with overall maximum improvement in all motor symptoms lies in the superior-lateral portion of the STN.

This pattern could partly explain the disparity in the findings of previous reports exploring the best stimulation site. It is now apparent that improvement in different motor symptoms might be associated with stimulation of different sites in and around the STN. This is not a novel notion, Cintas and colleagues showed that improvement in tremor, rigidity and bradykinesia can follow stimulation in different contacts (Cintas et al., 2003). Clusters corresponding to familiar side effects encountered with stimulation in well-established anatomical locations validate our findings (Figure2).

It is paramount to highlight that the stimulation effect presented (for efficacy and side-effects) is a response to acute stimulation (during screening) and not long-term stimulation. This is an especially important point with regard to delayed emergence of side-effects resulting from chronic stimulation, particularly deterioration in speech intelligibility. The optimal DBS target may eventually vary according to emergence of such side-effects (Plaha et al., 2008; Tripoliti et al., 2013).

There are two main problems of carrying out a group analysis examining efficacy of individual DBS contacts. The first is the variability in the STN between individuals (and hemispheres in the same individual) and the method to describe contact locations. Using categorical, arbitrary division within the nucleus reduces sensitivity and specificity of the analysis. It also introduces observer bias. We overcame this

problem by using a unique probabilistic STN template generated from our patient group, in order to visualise the resulting clusters, and co-registering volumes of tissue activation to MNI space. We tested voxels independently in the analysis across all contacts/ voltages for each individual, increasing the sensitivity and specificity of our approach.

The second problem is adjusting for baseline inhomogeneity. This is often overlooked and can produce statistical anomalies (e.g. a 5-point improvement from a baseline of 10 gives the same percentage of improvement of 30 from a baseline of 60) (Vickers, 2001; Zaidel et al., 2010). In order to overcome this, we examined efficacy clusters in each patient individually. The resultant clusters were then averaged across the entire group.

4.2 Tractography and cortical connectivity fingerprint

In vivo tractography studies in the region of the STN carry significant challenges. Motion artefacts, as a result of the highly pulsatile nature of the brainstem region, can degrade the MRI signal during diffusion image acquisition, reducing the signal-to-noise ratio (SNR). This is complicated by the presence of myriad criss-crossing axons and reticular brain regions (Lambert et al., 2013a; 2013b). One way of dealing with this is by using pulse-gating and respiratory rate monitoring during diffusion imaging. Likewise, by acquiring multiple diffusion scans, at a high angular resolution (increasing acquisition time), SNR is improved (Behrens et al., 2007; 2003).

Several studies have indeed used tractography to examine STN connectivity to cortical and subcortical areas but most used diffusion MR acquisition parameters more suited for conventional clinical application, such as mapping major white matter tracts prior to surgical intervention with low angular resolution (number of diffusion directions ≤ 64), low spatial resolution (voxel size $\geq$ 2mm) and low angular contrast (b-value=1000s/mm^2) (Aravamuthan et al., 2007; Avecillas-Chasin et al., 2016; Vanegas-Arroyave et al., 2016). Choosing the appropriate diffusion imaging parameters is of particular importance in the STN. This is in part due to its relatively small dimensions (12 mm in the longest axis and 4 mm in maximal thickness) (Schaltenbrand et al., 1977) requiring small voxel dimensions; and low fractional anisotropy (grey matter) requiring higher diffusion sensitisation (b-value).

We acquired 270 diffusion scans per patient (in 2×128 directions sets) over 62 minutes. We meticulously and systematically corrected artefacts and examined the processed imaging data for quality control. We modelled three crossing fibres per voxel and used probabilistic tractography to ameliorate the crossing fibre problem.

Recently, there has been a tendency to use tractography in an exploratory fashion. Though there is a place for this in delineating large white matter bundles, the results should always be scrutinised for false positives. Tunnel effect, crossing and kissing fibres pose particular difficulties (Behrens et al., 2007; Dyrby et al., 2007). In order to keep the analysis focused, a set of tractography rules based on knowledge from neurophysiological and NHP tracer studies was used, without being too restrictive. The effect of STN-cortical connectivity was examined rather than simply described. The precise role of the cortico-STN hyperdirect pathway remains to be fully understood. It has been proposed that, through this pathway, direct cortical information reaches the STN before indirect cortical output via the cortico-basal ganglia route. This potentially allows for direct cortical modulation of STN output (Rektor et al., 2015).

Our working hypothesis was that STN DBS exerted an effect through the hyperdirect pathway. The results suggest that ***three*** hyperdirect pathways connect the combined electrode stimulation area in and around the STN. Furthermore, distinct connectivity patterns predict response to DBS. Connectivity to M1 appears to predict improvement in tremor; to SMA predicts improvement in bradykinesia; and to both SMA and PFC for improvement in rigidity. Purely visualising the tractography results from the subthalamic region to the distinct cortical areas is not informative by itself, however; the GLM analysis, examining the relationship with efficacy, illustrates that connectivity is indeed relevant to a degree that is comparable to that of DBS voltage.

This model fits with functional and anatomical expectations. A non-human primate tracer study examining the hyperdirect pathway shows that M1 STN terminals occupy the dorsolateral portion of the STN; whilst SMA and PFC terminals are more medially located, with areas of overlap between M1 and SMA; and SMA and PFC (Haynes and Haber, 2013).

From a functional perspective; the primary motor area, SMA and PFC command sub-specialised roles in motor control. PET and SPECT studies have shown reduced metabolism in the PFC and SMA with Parkinson's disease progression (Eidelberg, 2009; Huang et al., 2007; Ma et al., 2007). The SMA is typically concerned with

motor encoding and planning, whereas M1 is implicated with motor execution and the PFC plays a role in cognitive/ behavioural motor response selection and proactive motor inhibition (Jahanshahi et al., 2015a; 2015b; I. Obeso et al., 2013a). DBS of the STN, by impacting on different fronto-basal ganglia pathways, has been shown to produce differential effects on reactive and proactive inhibition and on conflict resolution (I. Obeso et al., 2013b).

Resting tremor in Parkinson's disease is thought to be pathologically separate from bradykinesia and rigidity. The severity and magnitude of tremor is not related to the amount of dopamine deficiency in the substantia nigra and response to dopamine replacement can be poor in comparison to response in other motor symptoms (Bostan et al., 2010; Hallett, 2012; Ni et al., 2010; Timmermann et al., 2003). Pathological oscillations in a cerebello-thalamo-cortical network, possibly triggered by pallidal dysfunction in Parkinson's disease, is thought to be culpable (Helmich et al., 2011). The cortical focus in this tremor network is in the primary motor cortex and not the SMA. This is supported by evidence from a transcranial magnetic stimulation (TMS) study that demonstrated tremor suppression following stimulation of the primary motor cortex (Ni et al., 2010).

A resting state functional MRI study has also shown increase in connectivity between the STN and hand area of M1 and the primary sensory cortex tremor-dominant subgroup; conversely, in a non-tremor subgroup, increased connectivity was found between the STN and wider cortical areas including the SMA as well as M1 (Baudrexel et al., 2011). Another study that used resting state fMRI showed that STN DBS modulates the hyperdirect M1-STN projections (Kahan et al., 2014).

Two confounding factors are present when testing cortical connectivity of the volumes of tissue activated around each contact. The increase in tissue volume leads to an increase in the number of tractography voxel seeds. This, in turn, increases the number of streamlines from the VTA to the cortex in a non-linear fashion. The second confounding factor arises from the inexact relationship between stimulation amplitudes and increasing efficacy. Especially because the local population of neurons may have different action-potential thresholds. For this reason, voltage and seed volume effects were made covariates to study their effect on efficacy as well as that of the connectivity profile.

In the case of rigidity, an upward trend for all voltages was noted, particularly for low/medium voltages (e.g. 2 and 3 Volts) with higher connectivity to PFC and SMA,

resulting in higher efficacy. For bradykinesia, the plot shows no clear trend for high voltages (3 and 4) but an upward trend for low voltages (1 and 2 Volts). In other words, when voltage is low, it matters most where the STN is stimulated. The tremor plot shows that voltage clearly determines efficacy in this case with a slight upward trend for voltages 1 and 3.

We focused the tractography analysis on hyperdirect pathways to three cortical areas known to be involved in tone control, motor initiation, planning and execution. We cannot rule out the existence of other cortical-STN pathways that may also influence outcome from DBS. Our analysis did not explore the influence of STN-subcortical connectivity (e.g. thalamic/ striatal). The reason for this is two-fold: the strength of tractography diminishes with distance rendering DBS-subcortical connectivity artificially stronger than DBS-cortical connectivity; and the combined VTA area ***clearly*** encroaches on the thalamic border as shown in Figure1. It is, therefore, hardly surprising to find an increase in connectivity between volumes of tissue activated and the thalamus, as was demonstrated in a recent study (Vanegas-Arroyave et al., 2016).

The efficacy cluster analysis we carried out does not address potential covariance within symptoms per se. We therefore cannot assert that the three areas are independent of each other based on the VBM analysis alone (especially in the case of rigidity and bradykinesia clusters), however; there is a clear difference in cortical connectivity pattern predictive of improvement in individual symptoms. This difference is supported by anatomical and functional studies as described in the discussion. We show that the average cluster lies in the dorsal-lateral portion of the STN in keeping with existing wisdom. We opted not to explore this relationship between the individual clusters further as this has little significance in clinical practice, as a well-placed DBS electrode can easily straddle the three areas. Nevertheless, carrying out the VBM analysis separately has produced convergent efficacy clusters in close proximity. This substantiates the novel technique used here.

4.3 Limitations

In this study, a patient specific, finite element model is used to create DBS-VTAs (Åström et al., 2008). This is a simplified linear model that does not account for local impedance inhomogeneity (Howell and McIntyre, 2017). While it is important efforts are put into improving DBS models to resemble reality, it may not help to add details

to a rough model when the basic knowledge of the DBS mechanisms of actions are still debated. Indeed, various models over- or under-estimate the VTA (Maks et al., 2009). The presence of axons of different diameters and cell bodies, with variable action-potential thresholds, in the DBS region, complicates matters further. Our other justification for not using a more ***complex*** model is the fact that minute variations in VTAs are unlikely to have a large effect on statistical analysis and tractography results, due to the relatively larger spatial resolution of our structural and diffusion MRI data. Although the number of patients was relatively small (20 for the analysis of bradykinesia and rigidity analysis and 14 for the tremor analysis), we analysed two cerebral hemispheres independently by investigating hemi-body effects of stimulation doubling up the overall number in the analysis. Furthermore, testing the effect of stimulation for each individual contact at different voltages provided more data points per hemisphere. The main reason for the relatively small number of subjects stems from the difficulty in recruiting patients with advanced Parkinson's disease who are successfully selected for STN-DBS and can also tolerate having a lengthy MRI scan. We assessed stimulation efficacy in the upper limbs and not the lower limbs. We judged that this would give a more quantifiable and reproducible measure of improvement. Furthermore, patients with significant lower limb symptoms are seldom good candidates for STN-DBS. This does however mean that our results concerning the efficacy spots cannot directly be transferrable to patients with lower limb symptoms.

Another limitation is the inherent diffusion MRI imperfections as detailed in the discussion. Further improvements in diffusion imaging, with higher spatial and angular resolution and improved MRI gradients will add to the value of this modality (Jbabdi and Johansen-Berg, 2011; Sotiropoulos et al., 2013).

Multiple registration steps introduce error to the system. Nonetheless; we meticulously confirmed registration accuracy at each step to alleviate the impact of this issue. Manual STN delineation introduces observer bias; however, using two experienced clinicians to perform this independently reduced inaccuracy. Furthermore, by using a group average imprecisions were minimized. Prior to carrying out the VTA cluster analysis, we lateralized the right sided DBS contacts and STN to the left. This approach is commonly used in imaging studies; however, it assumes no functional differences between the left and right STN. Given that the lateralised structures differ in size in our right hand dominant cohort, we must

acknowledge the possible existence of different connectivity and efficacy relationships according to STN laterality. However, although reports have pointed to the existence of lateralised differences in emotional processing, no such differences have been established in motor processing (Eitan et al., 2013).

Another limitation in the efficacy and side effect cluster analysis is the autocorrelation in the data. The VTAs, by definition, have a degree of overlap which increases the power but theoretically also increases the risk of false positives. This is certainly a weakness of the analysis. Having said that, spatial autocorrelation is a well-known phenomenon in VBM and fMRI analysis and permutation tests do not easily accommodate correlated datasets, as such dependence violates null-hypothesis exchangeability, however; it is suggested that non-parametric permutation testing is less amenable to false positives than parametric permutations (Kriegeskorte et al., 2008). We have also carried out the analysis for each subject separately to reduce the effect of inter-individual variability.

Lastly, the relatively long scan duration is a drawback. This was accepted to achieve the required SNR and resolution. However, novel MRI acquisition techniques (Simultaneous Multi-Slice Imaging and Multi-Band Imaging) (Feinberg and Setsompop, 2013) have been developed that will allow future studies to run similar protocols within half the time without compromising the SNR.

5 Conclusion

The optimal DBS site for patients with Parkinson's disease for tremor, bradykinesia and rigidity appears to correspond to different areas in the motor STN. Stimulation in the central portion of the superior STN is most effective for tremor, whilst stimulation in further medial and posterior areas, within the superior portion, gives highest improvements in bradykinesia and rigidity. DBS-cortical connectivity, along the hyperdirect pathways, to M1 is predictive of maximum improvement in tremor, to SMA is predictive of maximum improvement in bradykinesia and to both SMA and PFC is predictive of maximum improvement in rigidity.

6 Acknowledgements

We thank Rutger Nijlunsing, Jonas Roothans and Mattias Åström from Medtronic Eindhoven Design Center, The Netherlands for their help in providing and setting up the SureTune system that was used in this study.

7 Funding

This study was funded by a grant from the Brain Research Trust (BRT) and supported by researchers at the National Institute for Health Research University College London Hospitals Biomedical Research Centre. The Unit of Functional Neurosurgery, UCL Institute of Neurology, Queen Square, London is also supported by the Parkinson's Appeal and the Sainsbury Monument Trust. The Wellcome Trust Centre for Neuroimaging is supported by core funding from the Wellcome Trust (grant reference 091593/Z/10/Z). SJ is supported by Medical Research Council (MRC) (grant reference MR/L009013/1). SS is supported by EPSRC (EP/L023067/1).

8 Figure legend

Table 1: Patient demographics, preoperative L-DOPA challenge, postoperative change in UPDRS III and medication requirement

*: At surgery; **: At 12 months; ŧ: 2-tailed paired-t test; CI: Confidence Interval; Med: Medications; SD: Standard deviation; SE: Standard error; df: degrees of freedom; LC: L-DOPA Challenge (preoperative); LEDD: L-DOPA equivalent daily dose

Table 2: Volume of tissue activated significant clusters with maximum effect and centre of gravity coordinates in MNI and corresponding AC-PC space

VTA: Volume of tissue activation; VOL: Volume; P-VAL: p-value; AC: anterior commissure; PC: posterior commissure

Table 3. Model parameters that significantly contribute to the efficacy prediction.

P values correspond to testing each parameter being different from zero.

Con: connectivity

Figure 1: STN and VTA modelling, co-registration and analysis pathways
The graph on the left shows examples of STN, DBS lead and VTA modelling in SureTune package. Transformation from native space to MNI space is shown for STN and VTA models. Tractography to M1 is shown in red, to SMA in blue and to PFC in green. The graph on the right shows group average STN in green and total VTA area in red-yellow (IC: internal capsule; PFC: prefrontal cortex; SMA: supplementary motor area; M1: primary motor area; VTA: volume of tissue activated)

Figure 2: Volume of tissue activated significant clusters for maximum efficacy and emergence of side effects of subthalamic nucleus deep brain stimulation (z coordinate is in MNI space) Group average STN is shown in green

Figure 3: Volume of tissue activated significant clusters of subthalamic nucleus deep brain stimulation (MNI–Z = -7mm) *
*Group average STN is shown in green. All clusters were corrected for multiple comparisons using non-parametric (gold-standard) approaches

Figure 4: Group average tractography: from the combined overall average VTA mask– left and from the combined efficacy clusters - right to M1 (red), SMA (blue) and PFC (green)

Figure 5: Plots showing relationship between percentage improvement in efficacy and VTA-cortical connectivity with stimulation amplitude (right) for rigidity, bradykinesia and tremor. The connectivity of all voxels belonging to the respective VTA vs efficacy is illustrated with the scatter plots on the left. The median of these connectivity values is plotted vs efficacy on the right. Connectivity is defined as a t-score between the normalized streamline count of the activated STN region and the streamline count of the non-activated STN region, i.e. the latter is used as a "baseline" connectivity in each case.

9 References

Alexander, G.E., Crutcher, M.D., 1990. Functional architecture of basal ganglia

circuits: neural substrates of parallel processing. Trends in Neurosciences 13, 266–271.

Alexander, G.E., Crutcher, M.D., DeLong, M.R., 1990. Basal ganglia-thalamocortical circuits: parallel substrates for motor, oculomotor, "prefrontal" and “limbic” functions. Prog. Brain Res. 85, 119–146.

Andersson, J.L.R., Jenkinson, M., Smith, S., 2007. Non-linear registration aka Spatial normalisation [WWW Document]. URL http://www.fmrib.ox.ac.uk/analysis/techrep/tr07ja2/tr07ja2.pdf (accessed 5.18.16).

Andersson, J.L.R., Skare, S., Ashburner, J., 2003. How to correct susceptibility distortions in spin-echo echo-planar images: application to diffusion tensor imaging. NeuroImage 20, 870–888. doi:10.1016/S1053-8119(03)00336-7

Andersson, J.L.R., Sotiropoulos, S.N., 2016. An integrated approach to correction for off-resonance effects and subject movement in diffusion MR imaging. NeuroImage 125, 1063–1078. doi:10.1016/j.neuroimage.2015.10.019

Aravamuthan, B.R., Muthusamy, K.A., Stein, J.F., Aziz, T.Z., Johansen-Berg, H., 2007. Topography of cortical and subcortical connections of the human pedunculopontine and subthalamic nuclei. NeuroImage 37, 694–705. doi:10.1016/j.neuroimage.2007.05.050

Avecillas-Chasin, J.M., Rascón-Ramírez, F., Barcia, J.A., 2016. Tractographical model of the cortico-basal ganglia and corticothalamic connections: Improving Our Understanding of Deep Brain Stimulation. Clin Anat 29, 481–492. doi:10.1002/ca.22689

Åström, M., Diczfalusy, E., Martens, H., Wårdell, K., 2015. Relationship between neural activation and electric field distribution during deep brain stimulation. IEEE Trans. Biomed. Eng. 62, 664–672. doi:10.1109/TBME.2014.2363494

Åström, M., Zrinzo, L.U., Tisch, S., Tripoliti, E., Hariz, M.I., Wårdell, K., 2008. Method for patient-specific finite element modeling and simulation of deep brain stimulation. Med Biol Eng Comput 47, 21–28. doi:10.1007/s11517-008-0411-2

Baudrexel, S., Witte, T., Seifried, C., Wegner, von, F., Beissner, F., Klein, J.C., Steinmetz, H., Deichmann, R., Roeper, J., Hilker, R., 2011. Resting state fMRI reveals increased subthalamic nucleus-motor cortex connectivity in Parkinson's disease. NeuroImage 55, 1728–1738. doi:10.1016/j.neuroimage.2011.01.017

Behrens, T.E.J., Berg, H.J., Jbabdi, S., Rushworth, M.F.S., Woolrich, M.W., 2007. Probabilistic diffusion tractography with multiple fibre orientations: What can we gain? NeuroImage 34, 144–155. doi:10.1016/j.neuroimage.2006.09.018

Behrens, T.E.J., Woolrich, M.W., Jenkinson, M., Johansen-Berg, H., Nunes, R.G., Clare, S., Matthews, P.M., Brady, J.M., Smith, S.M., 2003. Characterization and propagation of uncertainty in diffusion-weighted MR imaging. Magn. Reson. Med. 50, 1077–1088. doi:10.1002/mrm.10609

Bejjani, B.P., Dormont, D., Pidoux, B., Yelnik, J., Damier, P., Arnulf, I., Bonnet, A.M., Marsault, C., Agid, Y., Philippon, J., Cornu, P., 2000. Bilateral subthalamic stimulation for Parkinson's disease by using three-dimensional stereotactic magnetic resonance imaging and electrophysiological guidance. Journal of Neurosurgery 92, 615–625. doi:10.3171/jns.2000.92.4.0615

Bergman, H., Feingold, A., Nini, A., Raz, A., Slovin, H., Abeles, M., Vaadia, E., 1998. Physiological aspects of information processing in the basal ganglia of normal and parkinsonian primates. Trends in Neurosciences 21, 32–38.

Bostan, A.C., Dum, R.P., Strick, P.L., 2010. The basal ganglia communicate with the cerebellum. Proc. Natl. Acad. Sci. U.S.A. 107, 8452–8456. doi:10.1073/pnas.1000496107

Brown, P., 2003. Oscillatory nature of human basal ganglia activity: relationship to the pathophysiology of Parkinson's disease. Mov Disord. 18, 357–363. doi:10.1002/mds.10358

Brown, P., Oliviero, A., Mazzone, P., Insola, A., Tonali, P., Di Lazzaro, V., 2001. Dopamine dependency of oscillations between subthalamic nucleus and pallidum in Parkinson's disease. Journal of Neuroscience 21, 1033–1038.

Cho, Z.-H., Min, H.-K., Oh, S.-H., Han, J.-Y., Park, C.-W., Chi, J.-G., Kim, Y.-B., Paek, S.H., Lozano, A.M., Lee, K.H., 2010. Direct visualization of deep brain stimulation targets in Parkinson disease with the use of 7-tesla magnetic resonance imaging. Journal of Neurosurgery 113, 639–647. doi:10.3171/2010.3.JNS091385

Cintas, P., Simonetta-Moreau, M., Ory, F., Brefel Courbon, C., Fabre, N., Chaynes, P., Sabatier, J., Sol, J.C., Rascol, O., Berry, I., Lazorthes, Y., 2003. Deep brain stimulation for parkinson's disease: correlation between intraoperative subthalamic nucleus neurophysiology and most effective contacts. Stereotact Funct Neurosurg 80, 108–113.

Coenen, V.A., Prescher, A., Schmidt, T., Picozzi, P., Gielen, F.L.H., 2008. What is dorso-lateral in the subthalamic Nucleus (STN)?—a topographic and anatomical consideration on the ambiguous description of today's primary target for deep brain stimulation (DBS) surgery. Acta Neurochir 150, 1163–1165. doi:10.1007/s00701-008-0136-x

DeLong, M.R., 1990. Primate models of movement disorders of basal ganglia origin. Trends in Neurosciences 13, 281–285.

Dyrby, T.B., Søgaard, L.V., Parker, G.J., Alexander, D.C., Lind, N.M., Baaré, W.F.C., Hay-Schmidt, A., Eriksen, N., Pakkenberg, B., Paulson, O.B., Jelsing, J., 2007. Validation of in vitro probabilistic tractography. NeuroImage 37, 1267–1277. doi:10.1016/j.neuroimage.2007.06.022

Eidelberg, D., 2009. Metabolic brain networks in neurodegenerative disorders: a functional imaging approach. Trends in Neurosciences 32, 548–557. doi:10.1016/j.tins.2009.06.003

Eitan, R., Shamir, R.R., Linetsky, E., Rosenbluh, O., Moshel, S., Ben-Hur, T., Bergman, H., Israel, Z., 2013. Asymmetric right/left encoding of emotions in the human subthalamic nucleus. Front Syst Neurosci 7, 69. doi:10.3389/fnsys.2013.00069

Eusebio, A., Pogosyan, A., Wang, S., Averbeck, B., Gaynor, L.D., Cantiniaux, S., Witjas, T., Limousin, P., Azulay, J.P., Brown, P., 2009. Resonance in subthalamo-cortical circuits in Parkinson's disease. Brain 132, 2139–2150. doi:10.1093/brain/awp079

Feinberg, D.A., Setsompop, K., 2013. Ultra-fast MRI of the human brain with simultaneous multi-slice imaging. J. Magn. Reson. 229, 90–100. doi:10.1016/j.jmr.2013.02.002

Foltynie, T., Zrinzo, L., Martinez-Torres, I., Tripoliti, E., Petersen, E., Holl, E., Aviles-Olmos, I., Jahanshahi, M., Hariz, M., Limousin, P., 2011. MRI-guided STN DBS in Parkinson's disease without microelectrode recording: efficacy and safety. Journal of Neurology, Neurosurgery & Psychiatry 82, 358–363. doi:10.1136/jnnp.2010.205542

Garcia-Garcia, D., Guridi, J., Toledo, J.B., Alegre, M., Obeso, J.A., Rodriguez-Oroz, M.C., 2016. Stimulation sites in the subthalamic nucleus and clinical improvement in Parkinson's disease: a new approach for active contact localization. Journal of Neurosurgery 1–12. doi:10.3171/2015.9.JNS15868

Godinho, F., Thobois, S., Magnin, M., Guenot, M., Polo, G., Benatru, I., Xie, J.,

Salvetti, A., Garcia-Larrea, L., Broussolle, E., Mertens, P., 2006. Subthalamic nucleus stimulation in Parkinson's disease : anatomical and electrophysiological localization of active contacts. J Neurol 253, 1347–1355. doi:10.1007/s00415-006-0222-z

Grabner, G., Janke, A.L., Budge, M.M., Smith, D., Pruessner, J., Collins, D.L., 2006. Symmetric atlasing and model based segmentation: an application to the hippocampus in older adults. Med Image Comput Comput Assist Interv 9, 58–66.

Gradinaru, V., Mogri, M., Thompson, K.R., Henderson, J.M., Deisseroth, K., 2009. Optical deconstruction of parkinsonian neural circuitry. Science 324, 354–359. doi:10.1126/science.1167093

Hallett, M., 2012. Parkinson's disease tremor: pathophysiology. Parkinsonism and Related Disorders 18 Suppl 1, S85–6. doi:10.1016/S1353-8020(11)70027-X

Hamani, C., 2004. The subthalamic nucleus in the context of movement disorders. Brain 127, 4–20. doi:10.1093/brain/awh029

Hamel, W., Fietzek, U., Morsnowski, A., Schrader, B., Herzog, J., Weinert, D., Pfister, G., Müller, D., Volkmann, J., Deuschl, G., Mehdorn, H.M., 2003. Deep brain stimulation of the subthalamic nucleus in Parkinson's disease: evaluation of active electrode contacts. Journal of Neurology, Neurosurgery & Psychiatry 74, 1036–1046. doi:10.1136/jnnp.74.8.1036

Hammond, C., Bergman, H., Brown, P., 2007. Pathological synchronization in Parkinson's disease: networks, models and treatments. Trends in Neurosciences 30, 357–364. doi:10.1016/j.tins.2007.05.004

Hardman, C.D., Henderson, J.M., Finkelstein, D.I., Horne, M.K., Paxinos, G., Halliday, G.M., 2002. Comparison of the basal ganglia in rats, marmosets, macaques, baboons, and humans: Volume and neuronal number for the output, internal relay, and striatal modulating nuclei. J. Comp. Neurol. 445, 238–255. doi:10.1002/cne.10165

Haynes, W.I.A., Haber, S.N., 2013. The organization of prefrontal-subthalamic inputs in primates provides an anatomical substrate for both functional specificity and integration: implications for Basal Ganglia models and deep brain stimulation. Journal of Neuroscience 33, 4804–4814. doi:10.1523/JNEUROSCI.4674-12.2013

Helmich, R.C., Janssen, M.J.R., Oyen, W.J.G., Bloem, B.R., Toni, I., 2011. Pallidal dysfunction drives a cerebellothalamic circuit into Parkinson tremor. Ann Neurol. 69, 269–281. doi:10.1002/ana.22361

Hernandez, M., Guerrero, G.D., Cecilia, J.M., García, J.M., Inuggi, A., Jbabdi, S., Behrens, T.E.J., Sotiropoulos, S.N., 2013. Accelerating fibre orientation estimation from diffusion weighted magnetic resonance imaging using GPUs. PLoS ONE 8, e61892. doi:10.1371/journal.pone.0061892

Hernandez-Fernandez, M., Reguly, I., Giles, M., Jbabdi, S., Smith, S., Sotiropoulos, S., 2016. A fast and flexible toolbox for tracking brain connections in diffusion MRI datasets using GPUs, in:. Presented at the Organization for Human Brain Mapping (OHBM), Geneva, Switzerland.

Herzog, J., Fietzek, U., Hamel, W., Morsnowski, A., Steigerwald, F., Schrader, B., Weinert, D., Pfister, G., Müller, D., Mehdorn, H.M., Deuschl, G., Volkmann, J., 2004. Most effective stimulation site in subthalamic deep brain stimulation for Parkinson's disease. Mov Disord. 19, 1050–1054. doi:10.1002/mds.20056

Hirschmann, J., Özkurt, T.E., Butz, M., Homburger, M., Elben, S., Hartmann, C.J., Vesper, J., Wojtecki, L., Schnitzler, A., 2011. Distinct oscillatory STN-cortical loops revealed by simultaneous MEG and local field potential recordings in patients with Parkinson's disease. NeuroImage 55, 1159–1168. doi:10.1016/j.neuroimage.2010.11.063

Holl, E.M., Petersen, E.A., Foltynie, T., Martinez-Torres, I., Limousin, P., Hariz, M.I., Zrinzo, L., 2010. Improving Targeting in Image-Guided Frame-Based Deep Brain Stimulation. Neurosurgery 67, ons437–ons447. doi:10.1227/NEU.0b013e3181f7422a

Howell, B., McIntyre, C.C., 2017. Role of Soft-Tissue Heterogeneity in Computational Models of Deep Brain Stimulation. Brain Stimulation 10, 46–50. doi:10.1016/j.brs.2016.09.001

Huang, C., Tang, C., Feigin, A., Lesser, M., Ma, Y., Pourfar, M., Dhawan, V., Eidelberg, D., 2007. Changes in network activity with the progression of Parkinson's disease. Brain 130, 1834–1846. doi:10.1093/brain/awm086

Hughes, A.J., Daniel, S.E., Kilford, L., Lees, A.J., 1992. Accuracy of clinical diagnosis of idiopathic Parkinson's disease: a clinico-pathological study of 100 cases. Journal of Neurology, Neurosurgery & Psychiatry 55, 181–184. doi:10.1136/jnnp.55.3.181

Jahanshahi, M., Obeso, I., Baunez, C., Alegre, M., Krack, P., 2015a. Parkinson's disease, the subthalamic nucleus, inhibition, and impulsivity. Mov Disord. 30, 128–140. doi:10.1002/mds.26049

Jahanshahi, M., Obeso, I., Rothwell, J.C., Obeso, J.A., 2015b. A fronto-striato-subthalamic-pallidal network for goal-directed and habitual inhibition. Nat Rev Neurosci. doi:10.1038/nrn4038

Jbabdi, S., Johansen-Berg, H., 2011. Tractography: where do we go from here? Brain Connectivity 1, 169–183. doi:10.1089/brain.2011.0033

Jbabdi, S., Sotiropoulos, S.N., Savio, A.M., Graña, M., Behrens, T.E.J., 2012. Model-based analysis of multishell diffusion MR data for tractography: how to get over fitting problems. Magn. Reson. Med. 68, 1846–1855. doi:10.1002/mrm.24204

Jenkinson, M., Bannister, P., Brady, M., Smith, S., 2002. Improved optimization for the robust and accurate linear registration and motion correction of brain images. NeuroImage 17, 825–841.

Jenkinson, M., Smith, S., 2001. A global optimisation method for robust affine registration of brain images. Med Image Anal 5, 143–156.

Johnsen, E.L., Sunde, N., Mogensen, P.H., Østergaard, K., 2010. MRI verified STN stimulation site - gait improvement and clinical outcome. Eur J Neurol 17, 746–753. doi:10.1111/j.1468-1331.2010.02962.x

Kahan, J., Urner, M., Moran, R., Flandin, G., Marreiros, A., Mancini, L., White, M., Thornton, J., Yousry, T., Zrinzo, L., Hariz, M., Limousin, P., Friston, K., Foltynie, T., 2014. Resting state functional MRI in Parkinson's disease: the impact of deep brain stimulation on ‘effective’ connectivity. Brain 137, 1130–1144. doi:10.1093/brain/awu027

Kitai, S.T., Kita, H., 1987. Anatomy and Physiology of the Subthalamic Nucleus: A Driving Force of the Basal Ganglia, in: Carpenter, M.B., Jayaraman, A. (Eds.), The Basal Ganglia II: Structure and Function—Current Concepts, The Basal Ganglia II: Structure and Function—Current Concepts. Springer US, Boston, MA, pp. 357–373. doi:10.1007/978-1-4684-5347-8_25

Krack, P., Batir, A., Van Blercom, N., Chabardes, S., Fraix, V., Ardouin, C., Koudsie, A., Limousin, P.D., Benazzouz, A., LeBas, J.-F., Benabid, A.L., Pollak, P., 2003. Five-year follow-up of bilateral stimulation of the subthalamic nucleus in advanced Parkinson's disease. N Engl J Med 349, 1925–1934. doi:10.1056/NEJMoa035275

Kriegeskorte, N., Bodurka, J., Bandettini, P., 2008. Artifactual time-course correlations in echo-planar fMRI with implications for studies of brain function. International Journal of Imaging Systems and Technology 18, 345–349.

doi:10.1002/ima.20166
Lalo, E., Thobois, S., Sharott, A., Polo, G., Mertens, P., Pogosyan, A., Brown, P., 2008. Patterns of bidirectional communication between cortex and basal ganglia during movement in patients with Parkinson disease. Journal of Neuroscience 28, 3008–3016. doi:10.1523/JNEUROSCI.5295-07.2008
Lambert, C., Chowdhury, R., Fitzgerald, T.H.B., Fleming, S.M., Lutti, A., Hutton, C., Draganski, B., Frackowiak, R., Ashburner, J., 2013a. Characterizing aging in the human brainstem using quantitative multimodal MRI analysis. Front Hum Neurosci 7, 462. doi:10.3389/fnhum.2013.00462
Lambert, C., Lutti, A., Helms, G., Frackowiak, R., Ashburner, J., 2013b. Multiparametric brainstem segmentation using a modified multivariate mixture of Gaussians. Neuroimage Clin 2, 684–694. doi:10.1016/j.nicl.2013.04.017
Lambert, C., Zrinzo, L., Nagy, Z., Lutti, A., Hariz, M., Foltynie, T., Draganski, B., Ashburner, J., Frackowiak, R., 2012. Confirmation of functional zones within the human subthalamic nucleus: patterns of connectivity and sub-parcellation using diffusion weighted imaging. NeuroImage 60, 83–94. doi:10.1016/j.neuroimage.2011.11.082
Lanotte, M.M., Rizzone, M., Bergamasco, B., Faccani, G., Melcarne, A., Lopiano, L., 2002. Deep brain stimulation of the subthalamic nucleus: anatomical, neurophysiological, and outcome correlations with the effects of stimulation. Journal of Neurology, Neurosurgery & Psychiatry 72, 53–58. doi:10.1136/jnnp.72.1.53
Limousin, P., Pollak, P., Benazzouz, A., Hoffmann, D., Le Bas, J.-F., Broussolle, E., Perret, J.E., Benabid, A.L., 1995. Effect of parkinsonian signs and symptoms of bilateral subthalamic nucleus stimulation. The Lancet 345, 91–95.
Litvak, V., Jha, A., Eusebio, A., Oostenveld, R., Foltynie, T., Limousin, P., Zrinzo, L., Hariz, M.I., Friston, K., Brown, P., 2011. Resting oscillatory cortico-subthalamic connectivity in patients with Parkinson's disease. Brain 134, 359–374. doi:10.1093/brain/awq332
Lumsden, D.E., Ashmore, J., Charles-Edwards, G., Selway, R., Lin, J.-P., Ashkan, K., 2015. Observation and modeling of deep brain stimulation electrode depth in the pallidal target of the developing brain. WNEU 83, 438–446. doi:10.1016/j.wneu.2015.01.012
Ma, Y., Tang, C., Spetsieris, P.G., Dhawan, V., Eidelberg, D., 2007. Abnormal metabolic network activity in Parkinson's disease: test-retest reproducibility. J Cereb Blood Flow Metab 27, 597–605. doi:10.1038/sj.jcbfm.9600358
Maks, C.B., Butson, C.R., Walter, B.L., Vitek, J.L., McIntyre, C.C., 2009. Deep brain stimulation activation volumes and their association with neurophysiological mapping and therapeutic outcomes. Journal of Neurology, Neurosurgery & Psychiatry 80, 659–666. doi:10.1136/jnnp.2007.126219
Nakano, K., Hasegawa, Y., Tokushige, A., Nakagawa, S., Kayahara, T., Mizuno, N., 1990. Topographical projections from the thalamus, subthalamic nucleus and pedunculopontine tegmental nucleus to the striatum in the Japanese monkey, Macaca fuscata. Brain Research 537, 54–68.
Nambu, A., Takada, M., Inase, M., Tokuno, H., 1996. Dual somatotopical representations in the primate subthalamic nucleus: evidence for ordered but reversed body-map transformations from the primary motor cortex and the supplementary motor area. J. Neurosci. 16, 2671–2683.
Nambu, A., Tokuno, H., Inase, M., Takada, M., 1997. Corticosubthalamic input zones from forelimb representations of the dorsal and ventral divisions of the premotor cortex in the macaque monkey: comparison with the input zones from the primary

motor cortex and the supplementary motor area. Neuroscience Letters 239, 13–16.

Nambu, A., Tokuno, H., Takada, M., 2002. Functional significance of the cortico-subthalamo-pallidal "hyperdirect" pathway. Neuroscience Research 43, 111–117.

Ni, Z., Pinto, A.D., Lang, A.E., Chen, R., 2010. Involvement of the cerebellothalamocortical pathway in Parkinson disease. Ann Neurol. 68, 816–824. doi:10.1002/ana.22221

Obeso, I., Cho, S.S., Antonelli, F., Houle, S., Jahanshahi, M., Ko, J.H., Strafella, A.P., 2013a. Stimulation of the pre-SMA influences cerebral blood flow in frontal areas involved with inhibitory control of action. Brain Stimulation 6, 769–776. doi:10.1016/j.brs.2013.02.002

Obeso, I., Wilkinson, L., Rodriguez-Oroz, M.C., Obeso, J.A., Jahanshahi, M., 2013b. Bilateral stimulation of the subthalamic nucleus has differential effects on reactive and proactive inhibition and conflict-induced slowing in Parkinson's disease. Exp Brain Res 226, 451–462. doi:10.1007/s00221-013-3457-9

Obeso, J.A., Rodriguez-Oroz, M.C., Benitez-Temino, B., Blesa, F.J., Guridi, J., Marin, C., Rodriguez, M., 2008. Functional organization of the basal ganglia: therapeutic implications for Parkinson's disease. Mov Disord. 23 Suppl 3, S548–59. doi:10.1002/mds.22062

O'Gorman, R.L., Jarosz, J.M., Samuel, M., Clough, C., Selway, R.P., Ashkan, K., 2009. CT/MR image fusion in the postoperative assessment of electrodes implanted for deep brain stimulation. Stereotact Funct Neurosurg 87, 205–210. doi:10.1159/000225973

Parent, A., Hazrati, L.N., 1995. Functional anatomy of the basal ganglia. II. The place of subthalamic nucleus and external pallidum in basal ganglia circuitry. Brain Res. Brain Res. Rev. 20, 128–154.

Petersen, E.A., Holl, E.M., Martinez-Torres, I., Foltynie, T., Limousin, P., Hariz, M.I., Zrinzo, L., 2010. Minimizing brain shift in stereotactic functional neurosurgery. Neurosurgery 67, ons213–21– discussion ons221. doi:10.1227/01.NEU.0000380991.23444.08

Plaha, P., 2006. Stimulation of the caudal zona incerta is superior to stimulation of the subthalamic nucleus in improving contralateral parkinsonism. Brain 129, 1732–1747. doi:10.1093/brain/awl127

Plaha, P., Khan, S., Gill, S.S., 2008. Bilateral stimulation of the caudal zona incerta nucleus for tremor control. Journal of Neurology, Neurosurgery & Psychiatry 79, 504–513. doi:10.1136/jnnp.2006.112334

Rektor, I., Bočková, M., Chrastina, J., Rektorová, I., Baláž, M., 2015. The modulatory role of subthalamic nucleus in cognitive functions - a viewpoint. Clin Neurophysiol 126, 653–658. doi:10.1016/j.clinph.2014.10.156

Schaltenbrand, G., Wahren, W., Hassler, R., 1977. Atlas for Stereotaxy of the Human Brain. Thieme Medical Publishers.

Schmidt, C., van Rienen, U., 2012. Modeling the field distribution in deep brain stimulation: the influence of anisotropy of brain tissue. IEEE Trans. Biomed. Eng. 59, 1583–1592. doi:10.1109/TBME.2012.2189885

Shimamoto, S.A., Ryapolova-Webb, E.S., Ostrem, J.L., Galifianakis, N.B., Miller, K.J., Starr, P.A., 2013. Subthalamic nucleus neurons are synchronized to primary motor cortex local field potentials in Parkinson's disease. Journal of Neuroscience 33, 7220–7233. doi:10.1523/JNEUROSCI.4676-12.2013

Smith, S.M., 2002. Fast robust automated brain extraction. Hum. Brain Mapp. 17, 143–155. doi:10.1002/hbm.10062

Smith, S.M., Jenkinson, M., Woolrich, M.W., Beckmann, C.F., Behrens, T.E.J.,

Johansen-Berg, H., Bannister, P.R., De Luca, M., Drobnjak, I., Flitney, D.E., Niazy, R.K., Saunders, J., Vickers, J., Zhang, Y., De Stefano, N., Brady, J.M., Matthews, P.M., 2004. Advances in functional and structural MR image analysis and implementation as FSL. NeuroImage 23 Suppl 1, S208–19. doi:10.1016/j.neuroimage.2004.07.051

Smith, S.M., Nichols, T.E., 2009. Threshold-free cluster enhancement: addressing problems of smoothing, threshold dependence and localisation in cluster inference. NeuroImage 44, 83–98. doi:10.1016/j.neuroimage.2008.03.061

Sotiropoulos, S.N., Jbabdi, S., Xu, J., Andersson, J.L., Moeller, S., Auerbach, E.J., Glasser, M.F., Hernandez, M., Sapiro, G., Jenkinson, M., Feinberg, D.A., Yacoub, E., Lenglet, C., Van Essen, D.C., Ugurbil, K., Behrens, T.E.J., WU-Minn HCP Consortium, 2013. Advances in diffusion MRI acquisition and processing in the Human Connectome Project. NeuroImage 80, 125–143. doi:10.1016/j.neuroimage.2013.05.057

Sotiropoulos, S.N., Steinmetz, P.N., 2007. Assessing the direct effects of deep brain stimulation using embedded axon models. J. Neural Eng. 4, 107–119. doi:10.1088/1741-2560/4/2/011

Timmermann, L., Gross, J., Dirks, M., Volkmann, J., Freund, H.-J., Schnitzler, A., 2003. The cerebral oscillatory network of parkinsonian resting tremor. Brain 126, 199–212.

Tripoliti, E., Akram, H., Holl, E., 2013. A Subtle Change In MRI-verified Targeting Significantly Improves Long-term Speech Outcome After STN-DBS. ….

Vanegas-Arroyave, N., Lauro, P.M., Huang, L., Hallett, M., Horovitz, S.G., Zaghloul, K.A., Lungu, C., 2016. Tractography patterns of subthalamic nucleus deep brain stimulation. Brain 139, 1200–1210. doi:10.1093/brain/aww020

Vergani, F., Landi, A., Antonini, A., Parolin, M., Cilia, R., Grimaldi, M., Ferrarese, C., Gaini, S.M., Sganzerla, E.P., 2007. Anatomical identification of active contacts in subthalamic deep brain stimulation. Surgical Neurology 67, 140–146. doi:10.1016/j.surneu.2006.06.054

Vickers, A.J., 2001. The use of percentage change from baseline as an outcome in a controlled trial is statistically inefficient: a simulation study. BMC Med Res Methodol 1, 6. doi:10.1186/1471-2288-1-6

Voges, J., Volkmann, J., Allert, N., Lehrke, R., Koulousakis, A., Freund, H.-J., Sturm, V., 2002. Bilateral high-frequency stimulation in the subthalamic nucleus for the treatment of Parkinson disease: correlation of therapeutic effect with anatomical electrode position. Journal of Neurosurgery 96, 269–279. doi:10.3171/jns.2002.96.2.0269

Weise, L.M., Seifried, C., Eibach, S., Gasser, T., Roeper, J., Seifert, V., Hilker, R., 2013. Correlation of active contact positions with the electrophysiological and anatomical subdivisions of the subthalamic nucleus in deep brain stimulation. Stereotact Funct Neurosurg 91, 298–305. doi:10.1159/000345259

Williams, A., Gill, S., Varma, T., Jenkinson, C., Quinn, N., Mitchell, R., Scott, R., Ives, N., Rick, C., Daniels, J., Patel, S., Wheatley, K., PD SURG Collaborative Group, 2010. Deep brain stimulation plus best medical therapy versus best medical therapy alone for advanced Parkinson's disease (PD SURG trial): a randomised, open-label trial. The Lancet Neurology 9, 581–591. doi:10.1016/S1474-4422(10)70093-4

Williams, D., Tijssen, M., van Bruggen, G., Bosch, A., Insola, A., Di Lazzaro, V., Mazzone, P., Oliviero, A., Quartarone, A., Speelman, H., Brown, P., 2002. Dopamine-dependent changes in the functional connectivity between basal ganglia and cerebral cortex in humans. Brain 125, 1558–1569.

Winkler, A.M., Ridgway, G.R., Webster, M.A., Smith, S.M., Nichols, T.E., 2014. Permutation inference for the general linear model. NeuroImage 92, 381–397. doi:10.1016/j.neuroimage.2014.01.060

Wodarg, F., Herzog, J., Reese, R., Falk, D., Pinsker, M.O., Steigerwald, F., Jansen, O., Deuschl, G., Mehdorn, H.M., Volkmann, J., 2012. Stimulation site within the MRI-defined STN predicts postoperative motor outcome. Mov Disord. 27, 874–879. doi:10.1002/mds.25006

Yelnik, J., Bardinet, E., Dormont, D., Malandain, G., Ourselin, S., Tandé, D., Karachi, C., Ayache, N., Cornu, P., Agid, Y., 2007. A three-dimensional, histological and deformable atlas of the human basal ganglia. I. Atlas construction based on immunohistochemical and MRI data. NeuroImage 34, 618–638. doi:10.1016/j.neuroimage.2006.09.026

Yelnik, J., Damier, P., Demeret, S., Gervais, D., Bardinet, E., Bejjani, B.-P., François, C., Houeto, J.-L., Arnule, I., Dormont, D., Galanaud, D., Pidoux, B., Cornu, P., Agid, Y., 2003. Localization of stimulating electrodes in patients with Parkinson disease by using a three-dimensional atlas-magnetic resonance imaging coregistration method. Journal of Neurosurgery 99, 89–99. doi:10.3171/jns.2003.99.1.0089

Yokoyama, T., Sugiyama, K., Nishizawa, S., Yokota, N., Ohta, S., Akamine, S., Namba, H., 2001. The Optimal Stimulation Site for Chronic Stimulation of the Subthalamic Nucleus in Parkinson’s Disease. Stereotact Funct Neurosurg 77, 61–67. doi:10.1159/000064598

Zaidel, A., Bergman, H., Ritov, Y., MD, Z.I., 2010. Levodopa and subthalamic deep brain stimulation responses are not congruent. Mov Disord. 25, 2379–2386. doi:10.1002/mds.23294

Zhang, T.C., Grill, W.M., 2010. Modeling deep brain stimulation: point source approximation versus realistic representation of the electrode. J. Neural Eng. 7, 066009. doi:10.1088/1741-2560/7/6/066009

Zheng, Z., Zhang, Y.-Q., Li, J.-Y., Zhang, X.-H., Zhuang, P., Li, Y.-J., 2009. Subthalamic deep brain stimulation for Parkinson's disease: correlation of active contacts and electrophysiologically mapped subthalamic nucleus. Chin. Med. J. 122, 2419–2422.

Zonenshayn, M., Sterio, D., Kelly, P.J., Rezai, A.R., Beric, A., 2004. Location of the active contact within the subthalamic nucleus (STN) in the treatment of idiopathic Parkinson's disease. Surgical Neurology 62, 216–225. doi:10.1016/j.surneu.2003.09.039

Table 1: Patient demographics, preoperative L-DOPA challenge, postoperative change in UPDRS III and medication requirement

	Mean	SD	SE	Minimum	Maximum	Range
Age*	56.3	10.2	2.3	41	71	30
Disease duration*	11.2	4.3	1.0	4	22	18
Duration of motor fluctuations*	3.1	2.0	0.4	0	9	9
UPDRS III OFF (LC)	43.8	13.0	3.0	20	73	53
UPDRS III ON (LC)	17.4	9.9	2.3	4	42	38
UPDRS III Improvement (LC)	26.5	10.1	2.3	7	47	40
95% CI:21.6-31.3, t:11.4, df:18, p<0.0001ŧ	**(61%)**	**(15.8%)**	**(3.6%)**	**(33%)**	**(91%)**	**(58%)**
UPDRS III (OFF Med. OFF DBS) **	50.5	17.2	3.9	24	96	72
UPDRS III (OFF Med. ON DBS) **	27.1	12.5	3.0	14	51	37
UPDRS III Improvement**	23.4	12.8	3.1	8	45	37
95% CI:16.8-29.4, t:7.5, df:16, p<0.0001ŧ	**(46%)**	**(17.4%)**	**(4.2%)**	**(22%)**	**(73%)**	**(51%)**
UPDRS III ON Med. OFF DBS**	27.6	14.1	3.2	10	62	52
UPDRS III ON Med. ON DBS**	13.3	9.1	2.2	3	34	31
UPDRS III Improvement**	14.3	8.0	1.9	41	28	24
95% CI:10.4-18.3, t:7.6, df:17, p<0.0001ŧ	**(52%)**	**(17.4%)**	**(4.1%)**	**(9%)**	**(81%)**	**(62%)**
LEDD (Preoperative)	1365.6	509.8	114	540	2550	2010
LEDD (Postoperative)	770.6	306.6	68.6	320	1266	946
LEDD Reduction with DBS	595	203.2	45.4	220	1284	1064
95% CI: 386.3-803.8, t:6, df:19, p<0.0001ŧ	**(44%)**	**(39.9%)**	**(39.8%)**	**(40.7%)**	**(50.4%)**	**(52.9%)**

*: At surgery; **: At 12 months; ŧ: 2-tailed paired-t test; CI: Confidence Interval; Med: Medications; SD: Standard deviation; SE: Standard error; df: degrees of freedom; LC: L-DOPA Challenge (preoperative); LEDD: L-DOPA equivalent daily dose

Table 3. Model parameters that significantly contribute to the efficacy prediction.

	Con STN-M1 (b1>0)	Con STN-SMA (b2>0)	Con STN-PFC (b3>0)	Voltage (b4>0)	VTA-Volume (b5>0)
Rigidity	p=0.035	p=0.0006	p=0.005	p=10-6	p=0.02
Bradykinesia	p>0.05	p=0.005	p>0.05	p=0.001	p>0.05
Tremor	p=0.04	p>0.05	p>0.05	p=10-7	p>0.05

P values correspond to testing each parameter being different from zero.

Con: connectivity

Table 2: Volume of tissue activated significant clusters with maximum effect and centre of gravity coordinates in MNI and corresponding AC-PC space

VTA Cluster	VOL (mm^3)	P-VAL	Maximum effect coordinates MNI (AC-PC)			Centre of gravity coordinates MNI (AC-PC)		
			X	Y	Z	X	Y	Z
Rigidity	62	0.006	-9 (-8.5)	-13 (-1)	-7 (-3)	-11 (-10.5)	-15 (-3)	-7 (-3)
Bradykinesia	6	0.037	-11 (-10.5)	-14 (-2)	-7 (-3)	-11 (-10.5)	-14 (-2)	-7 (-3)
Tremor	11	0.014	-11 (-10.5)	-12 (0)	-6 (-2)	-12 (-11.5)	-12 (0)	-6 (-2)
Combined	26	-	-10 (-9.5)	-13 (-1)	-7 (-3)	-11 (-10.5)	-14 (-2)	-7 (-3)
Facial pulling	77	0.012	-11 (-10.5)	-19 (-7)	-1 (3)	-12 (-11.5)	-18 (-6)	-2 (2)
Dysarthria	149	0.002	-17 (-16.5)	-12 (0)	-5 (-1)	-15 (-14.5)	-11 (1)	-2 (2)
Diplopia	185	0.002	-7 (-6.5)	-12 (0)	-15 (-11)	-7 (-6.5)	-16 (-4)	-12 (-8)
Paraesthesia	475	0.002	-10 (-9.5)	-20 (-8)	-18 (-14)	-11 (-10.5)	-15 (-3)	-12 (-8)

VTA: Volume of tissue activation; VOL: Volume; P-VAL: p-value; AC: anterior commissure; PC: posterior commissure

Figure 1

Click here to download high resolution image

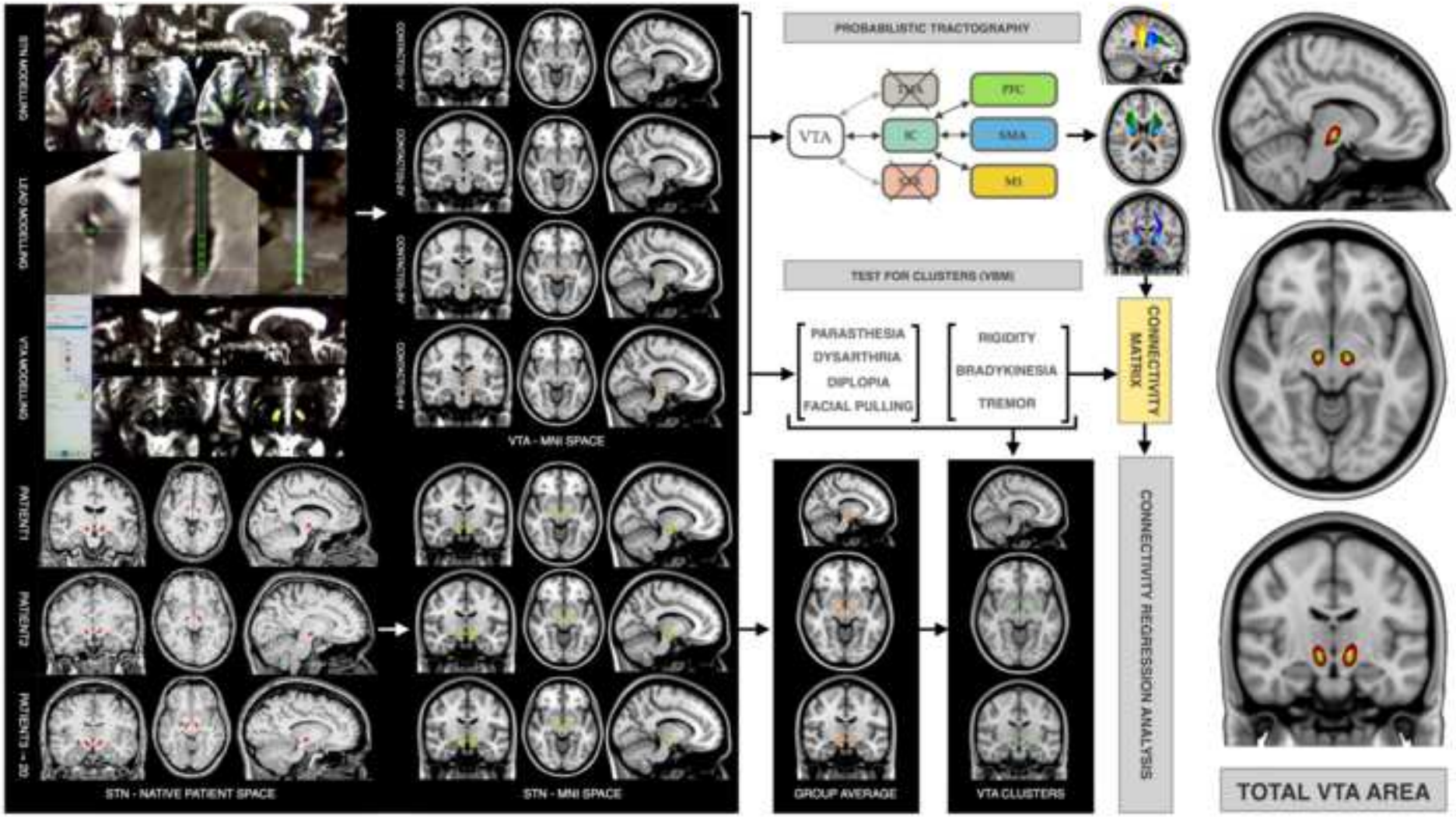

Figure 4

Click here to download high resolution image

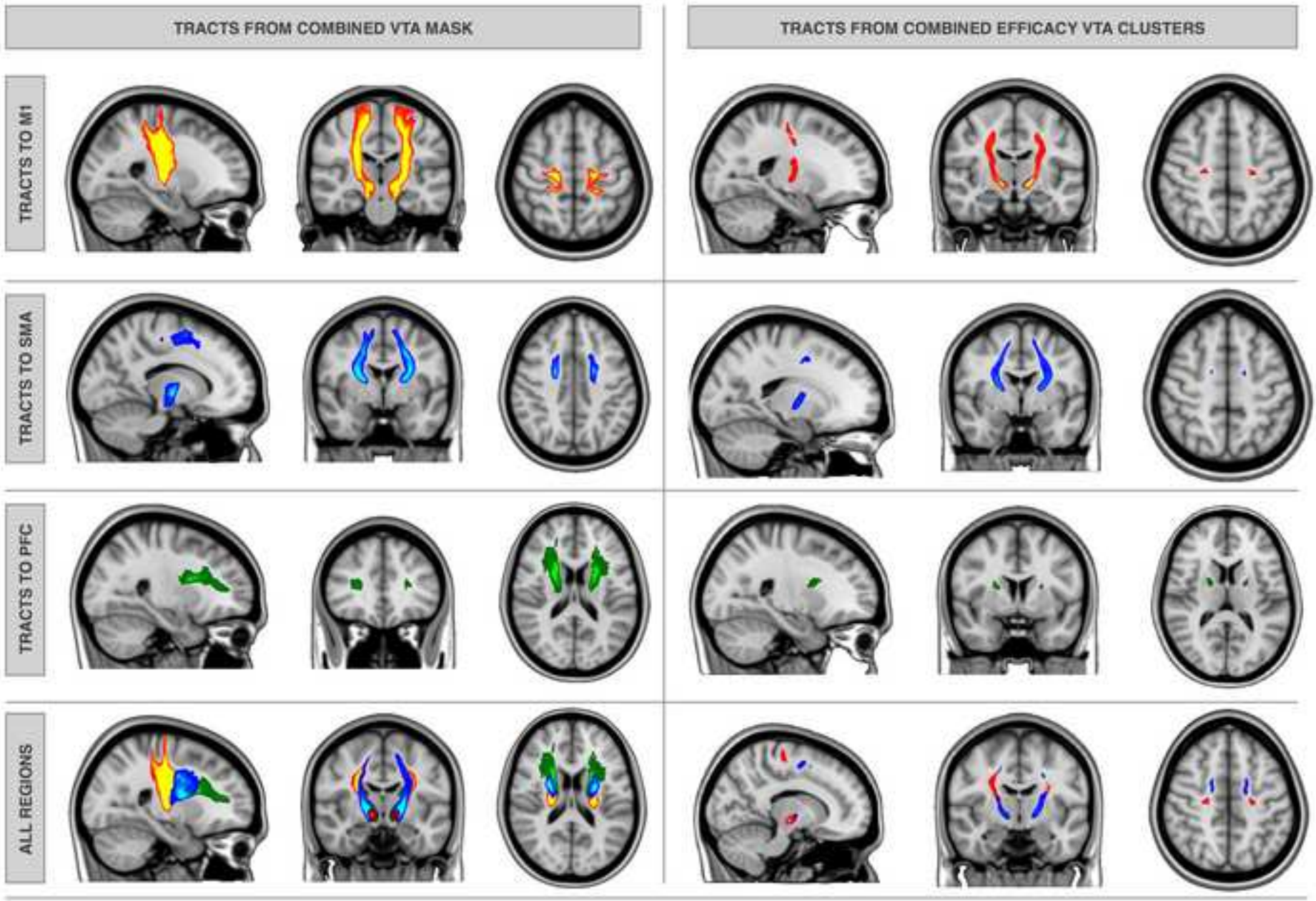

Figure 5

Click here to download high resolution image

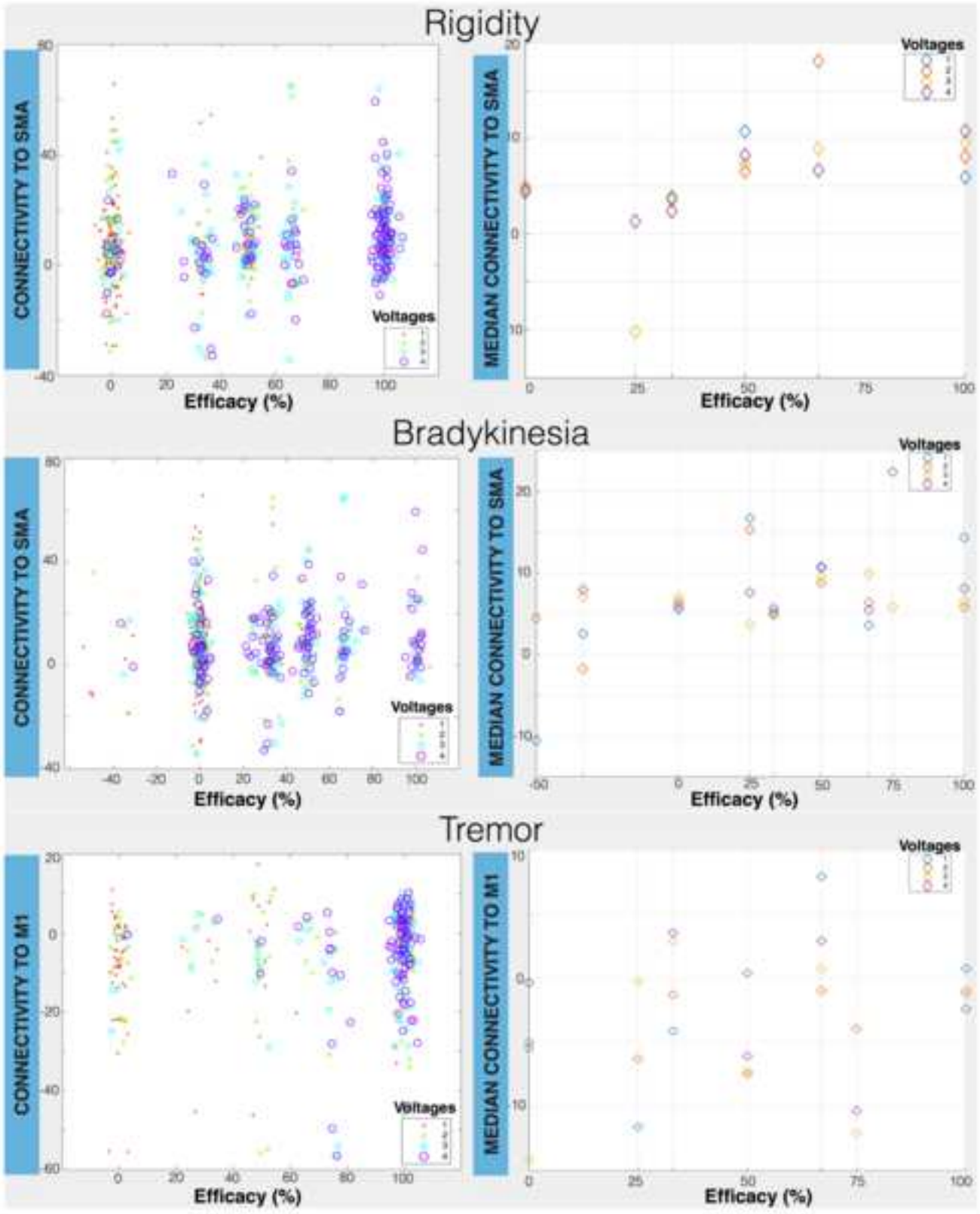

Figure 2

Click here to download high resolution image

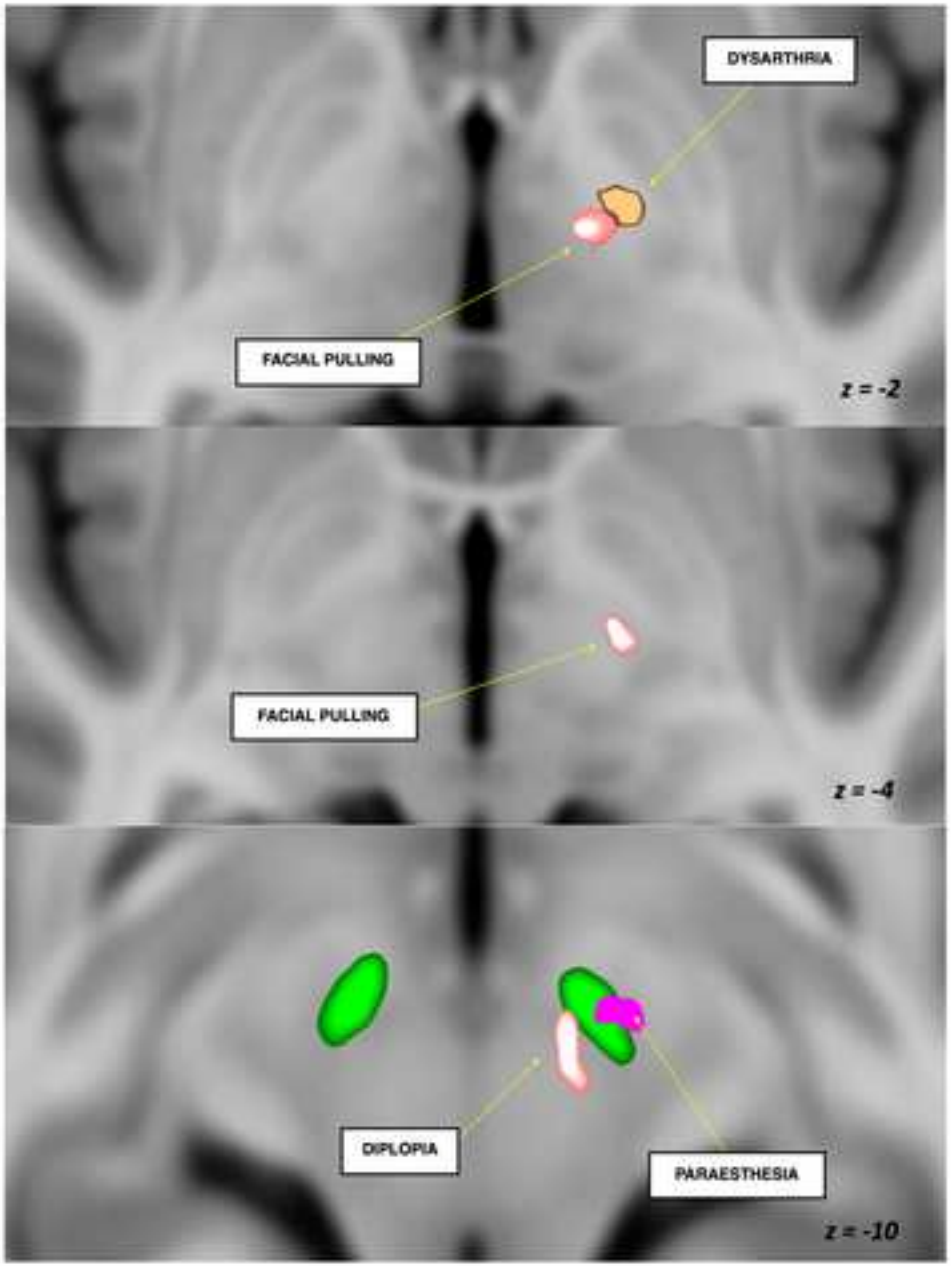

Figure 3

Click here to download high resolution image

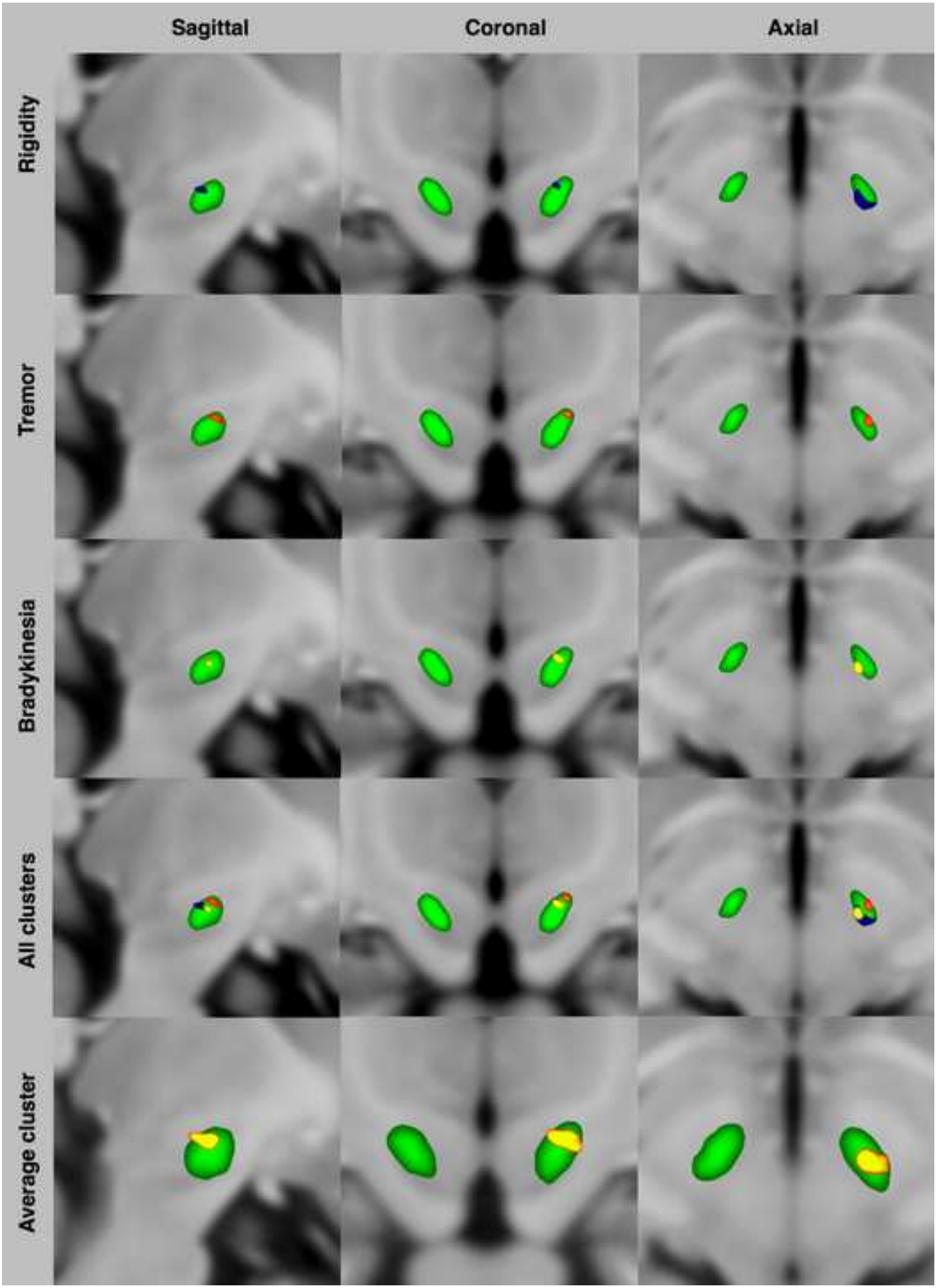

Supplementary Material

Click here to download 10. Supplementary Material: Supplementary material.doc